Electronic Supplementary Information (ESI) for:

A molecular porous zirconium-organic material exhibiting highly selective CO_2 adsorption, high thermal stability, reversible hydration, facile ligand exchanges, and exclusive dimerization of phenylacetylene

Nam Hee Lee,[1] Dong Woo Lee,[1] Hakmin Yeo,[1] Kyungwon Kwak,[1] Hyang Sook Chun,[2] and Kang Min Ok[1,*]

[1]*Department of Chemistry, Chung-Ang University, 84 Heukseok-ro, Dongjak-gu, Seoul 156-756, Korea*

[2]*School of Food Science and Technology, Chung-Ang University, Anseong, Gyeonggi 456-756, Republic of Korea*

E-mail: kmok@cau.ac.kr

CONTENTS

Figure S1. Calculated and observed powder X-ray diffraction patterns for CAUMOF-12

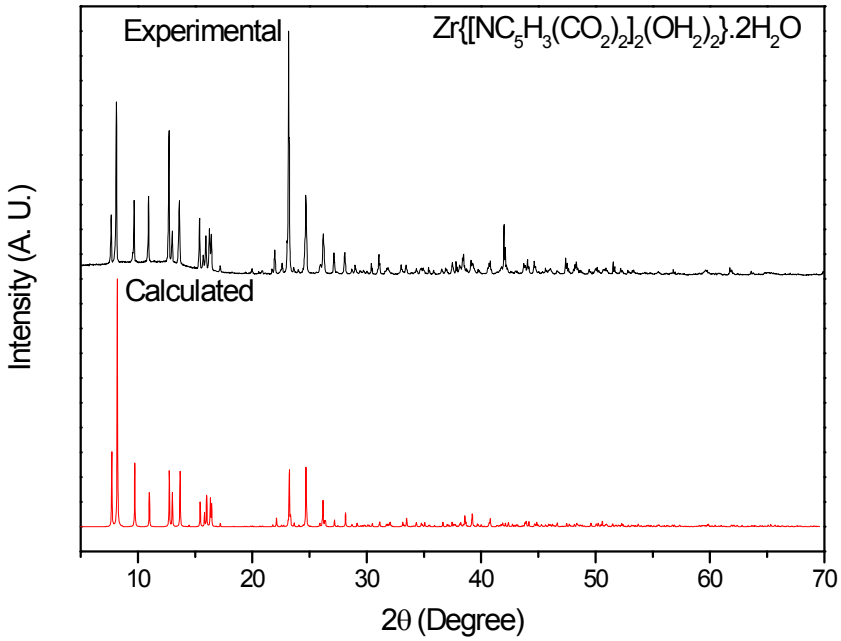

Figure S2. ^{1}H (600 MHz) and ^{13}C NMR (150 MHz) spectra for CAUMOF-12 measured in DMSO

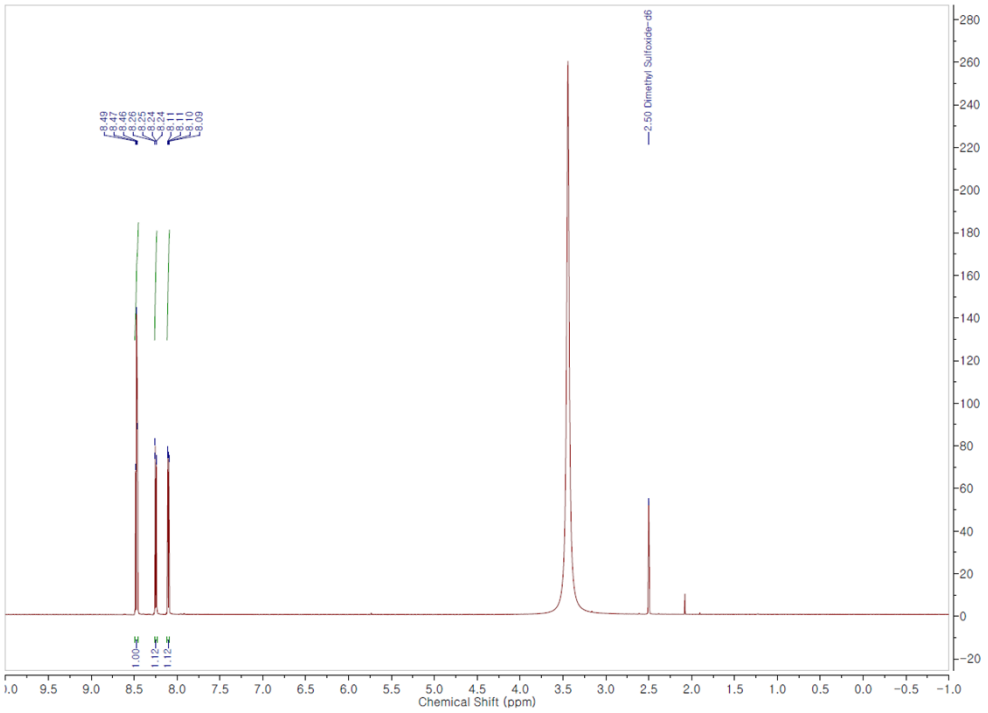

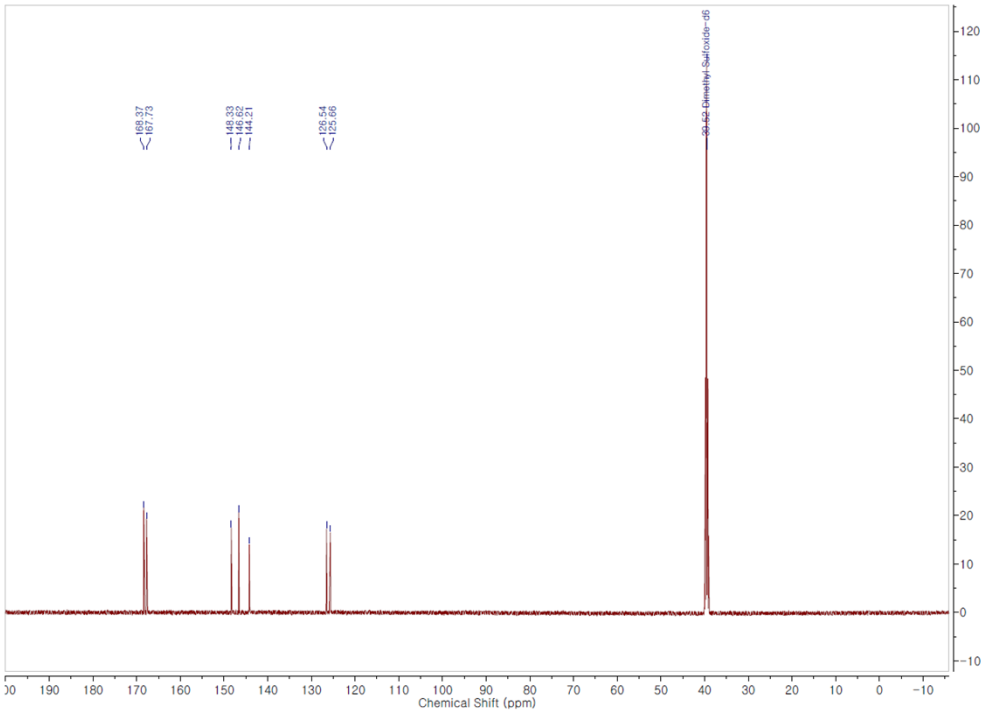

Figure S3. Infrared spectrum of CAUMOF-12

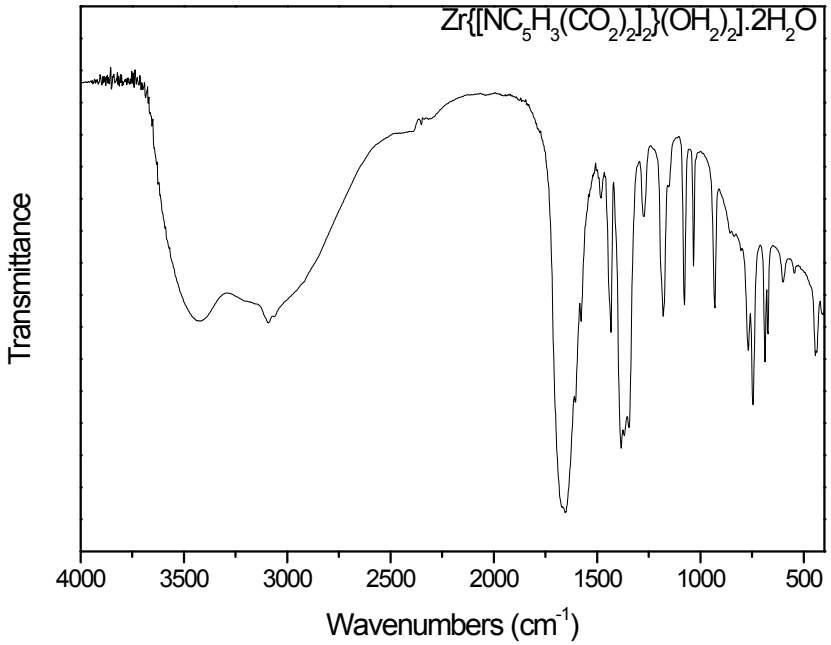

Figure S4. UV-Vis spectrum of CAUMOF-12

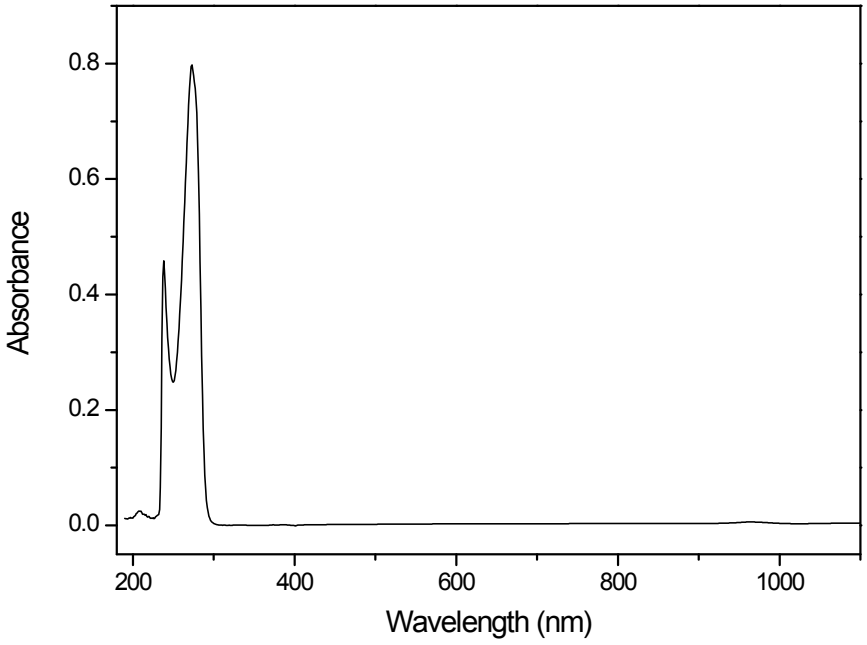

Figure S5. Pore size distribution plot for CAUMOF-12

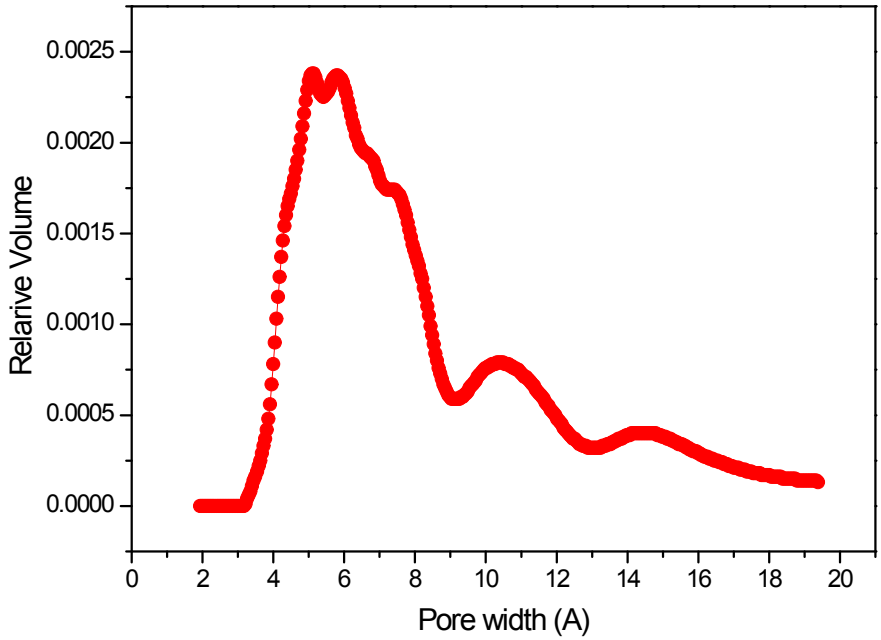

Pore size distribution has been calculated by SF method. Approximate pore diameters can be calculated to be 3–8 Å on the basis of CO_2 adsorption, which are in good agreement with the channel dimensions estimated from the single-crystal data.

Figure S6. ORTEP (50% probability ellipsoids) drawings of $Zr\{[NC_5H_3(CO_2)_2]_2(DMF)_2\}\cdot DMF$ and $Zr\{[NC_5H_3(CO_2)_2]_2(CH_3OH)_2\}\cdot CH_3OH$. Hydrogen atoms are omitted for clarity.

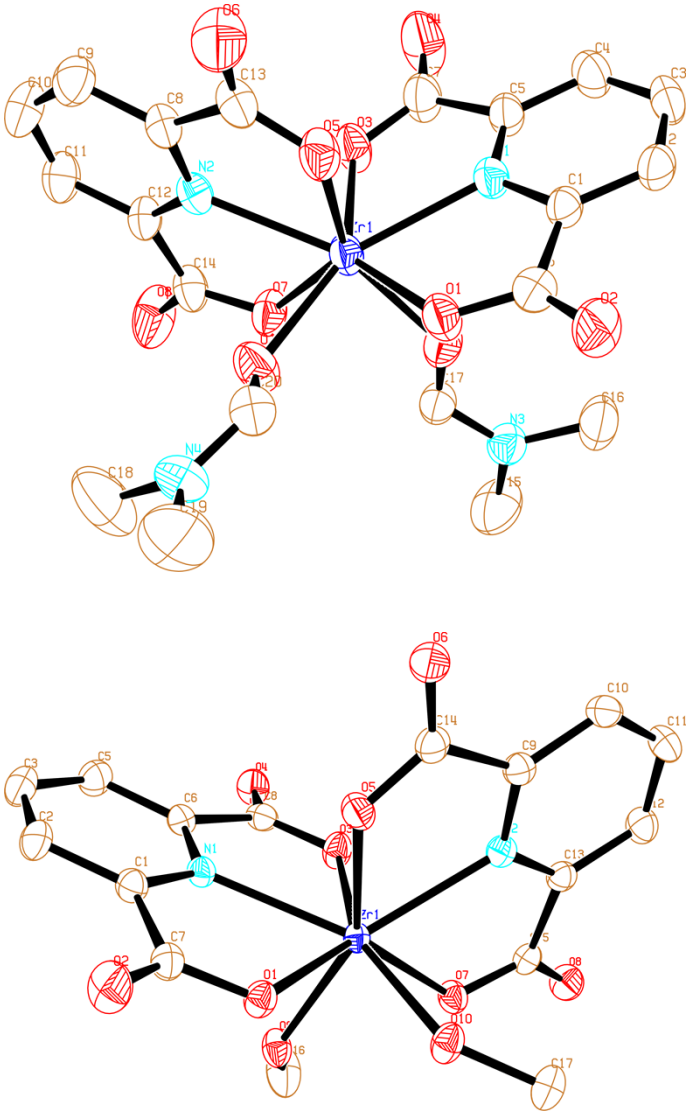

Figure S7. The band structure for CAUMOF-12 calculated with DMol[3]

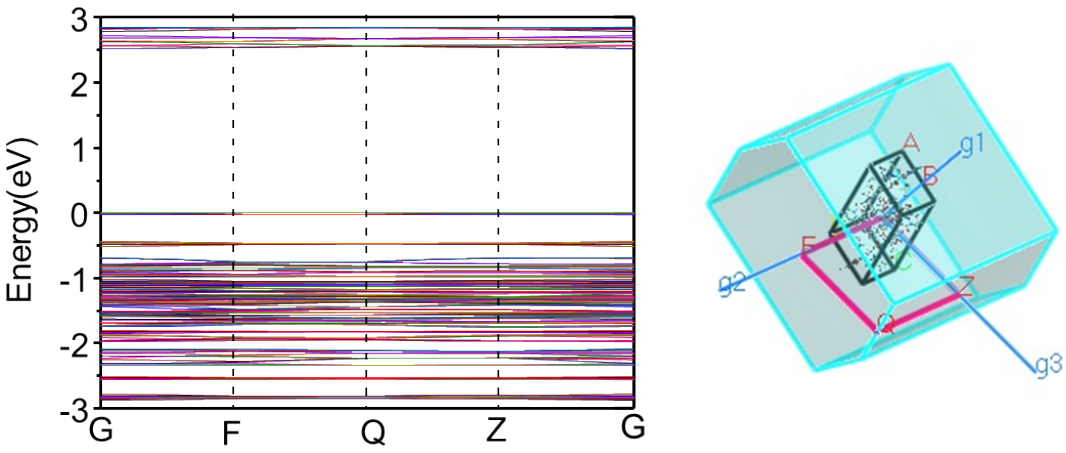

Figure S8. Gas Chromatograms for the dimerization and cyclotrimerization products of phenylacetylene with CAUMOF-12 at 110 °C and 180 °C

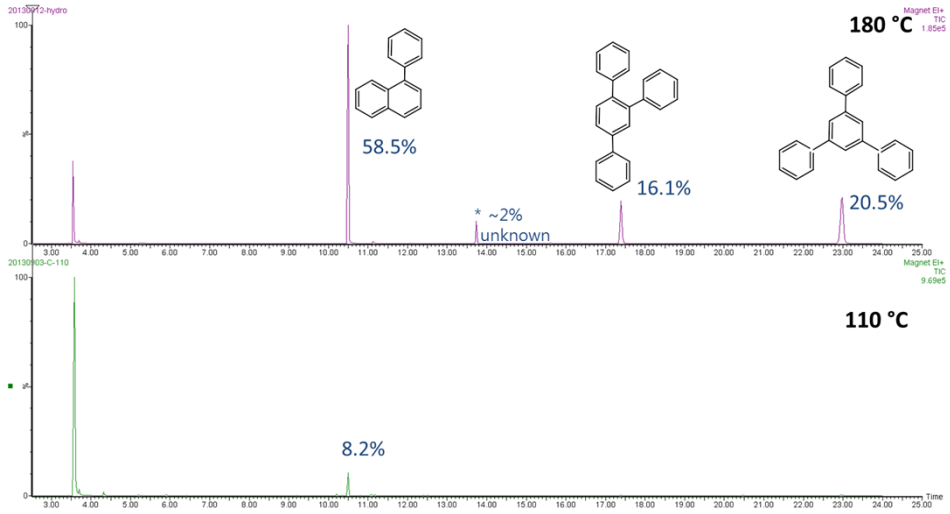

Figure S9. GC-Mass spectra for the dimerization and cyclotrimerization products of phenylacetylene with CAUMOF-12

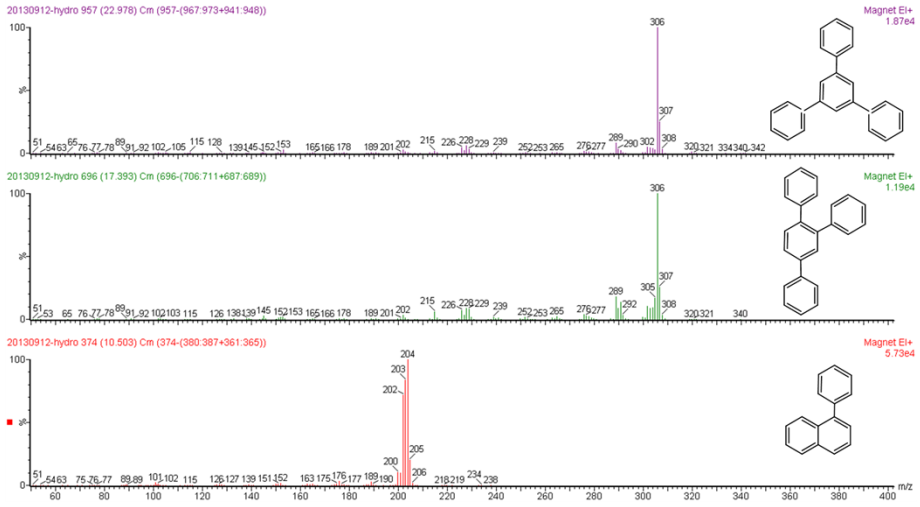

Figure S10. ^{1}H NMR (600 MHz) spectrum for the dimerization and cyclotrimerization products of phenylacetylene with CAUMOF-12

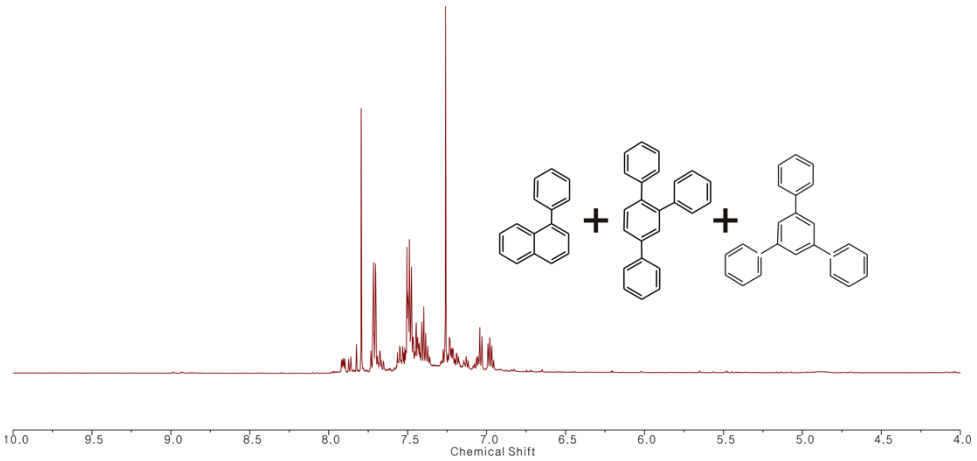

Figure S11. (a) Crystal structures of CAUMOF-12 determined from (a) X-ray diffraction, (b) DFT calculations, and (c) overlapped representation. (d) Wire model representing the two carboxylate groups in stacking ligands are in different environment.

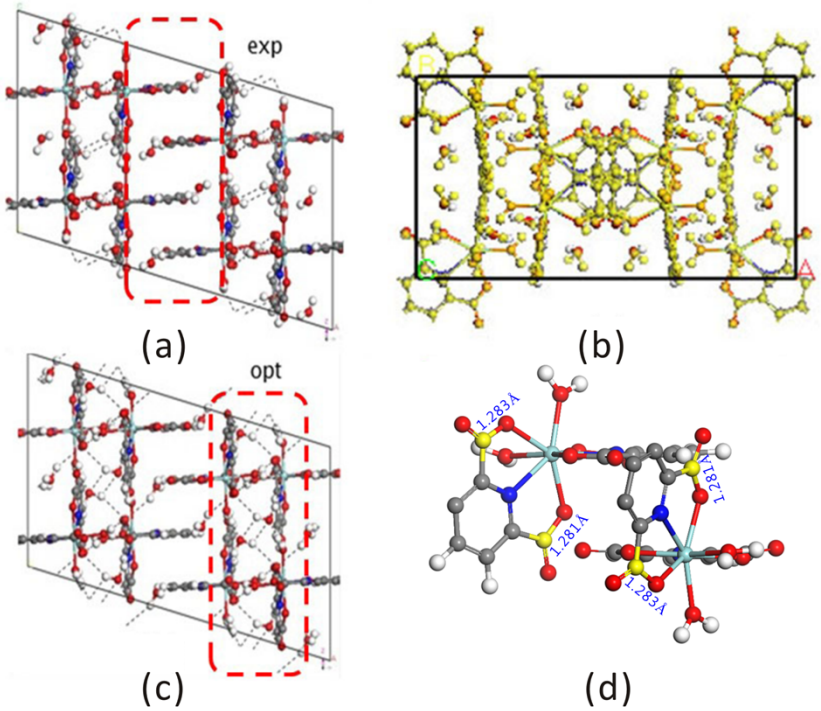

The experimentally determined crystal structure can be directly compared with the calculated structure. Figures S11a and b show structures of CAUMOF-12 determined from the experiment and DFT calculations, respectively. The dotted lines in the figure represent the hydrogen bonding interactions, and the two structures are overlapped with each other for a direct comparison (see Figure S11c). As seen in the overlapped image, all the atoms match quite well. For quantitative comparisons, bond distances determined from X-ray crystallography and DFT calculations are listed in Table S1. The ligand, 2,6-pyridinedicaboxylate, possesses a plane of symmetry. Thus, it is natural to expect the symmetric structure parameters against the plane. However, we found that some moieties of ligands adopt asymmetric environments attributed to interligand interactions, i.e., π–π interactions. Further, when the extended structure beyond the unit cell is investigated, various intermolecular interactions can be found between ligands. As seen in Figures S11a and b, both π–π stacking and hydrogen bonding interactions between adjacent ligands are observed, which results in different bond distances for the two ligands. We classify the two different moieties as stacking and non-stacking ligands and list detailed bond lengths in Table S1. From the experimental results, it is clear that the structures of stacking and non-stacking ligands are different as expected. Furthermore, when we compare the geometry of the two carboxylate groups in stacking ligands, clear asymmetric geometry around Zr atom and coordinating groups are found. To emphasize this asymmetry, the structure parameters are sorted as two groups, upper and lower rows. The upper and lower C–N bonds are quite different only in the stacking ligands as shown in the experimental result and the solid-state DFT calculations. In non-stacking ligands, however, upper and lower bond lengths show almost the same values. To confirm these asymmetric bond distances are caused by interligand interactions, we performed the geometry optimization with single Zr complex in gas phase. All structural changes are symmetric in gas phase calculations, although we can observe formation of the extended structure. To reveal the origin of this asymmetric structural change in the solid-state, we investigated the geometry around the stacking ligands more closely. As seen in Figure S11d, two carboxylate groups in stacking ligands are in quite different environments; only one carboxylate group can participate in π–π stacking with the neighboring carboxylate group from another complex. Most clear changes were observed from the lengths of C–O bonds; while chelating C–O bonds increase, non-chelating C–O bonds shorten when they are in stacking positions. These structural changes can be explained by the competitive delocalization of p orbitals of carbon atom. As the carbonyl group approaches, p orbitals of carbon and non-coordinating oxygen atoms start overlapping and make more population of π-electrons between the non-chelating carbonyl groups. This reduction of π-electrons along the C–O bond decreases the partial double bond character and elongates the bond lengths. It allows the close approach of the coordinating oxygen atom to the Zr center. Consequently, the π–π stacking introduces a distribution of Zr–O coordination length, which will break the symmetry around the Zr atom.

Table S1. Comparison of bond distances (Å) obtained from experimental data and optimized geometrical parameters using DFT calculations for CAUMOF-12

Atom	X-ray Crystallography		Single molecule DFT		Solid-State DFT	
	Stacking	Non-stacking	Free ligand	Zr complex	Stacking	Non-stacking
C(1)–N(1)	1.337(7)	1.333(4)	1.319	1.333	1.340	1.336
C(1)–C(6)	1.469(8)	1.492(4)	1.500	1.516	1.497	1.494
C(6)–O(4)	1.254(7)	1.234(3)	1.227	1.208	1.262	1.246
C(6)–O(3)	1.270(7)	1.281(3)	1.273	1.320	1.279	1.296
Zr(1)–O(3)	2.212(4)	2.162(3)	-	2.188	2.286	2.217
C(5)–N(1)	1.343(7)	1.335(4)	1.319	1.332	1.337	1.337
C(5)–C(7)	1.504(9)	1.497(3)	1.500	1.518	1.512	1.495
C(7)–O(6)	1.208(7)	1.234(4)	1.227	1.206	1.226	1.247
C(7)–O(5)	1.296(7)	1.283(4)	1.273	1.320	1.321	1.297
Zr(1)–O(5)	2.130(4)	2.188(2)	-	2.104	2.151	2.262
Zr(1)–N(1)	2.309(5)	2.304(2)	-	2.321	2.326	2.334